

THE PRIMARY PROTON SPECTRUM OF COSMIC RAYS MEASURED WITH SINGLE HADRONS AT GROUND LEVEL

T. ANTONI,¹ W. D. APEL,² F. BAEDA,^{2,3} K. BEKK,² A. BERCU,^{2,3} H. BLÜMER,^{1,2} H. BOZDOG,² I. M. BRANCUS,⁴ C. BÜTTNER,¹ A. CHILINGARIAN,⁵ K. DAUMILLER,¹ P. DOLL,² R. ENGEL,² J. ENGLER,² F. FEßLER,² H. J. GILS,² R. GLASSTETTER,^{1,6} A. HAUNGS,² D. HECK,² J. R. HÖRANDEL,¹ K.-H. KAMPERT,^{1,2,6} H. O. KLAGES,² G. MAIER,² H. J. MATHES,² H. J. MAYER,² J. MILKE,² M. MÜLLER,^{2,7} R. OBENLAND,² J. OEHLSCHLÄGER,² S. OSTAPCHENKO,^{1,8} M. PETCU,⁴ H. REBEL,² A. RISSE,⁹ M. RISSE,² M. ROTH,¹ G. SCHATZ,² H. SCHIELER,² J. SCHOLZ,² T. THOUW,² H. ULRICH,² J. VAN BUREN,² A. VARDANYAN,⁵ A. WEINDL,² J. WOCHELE,² AND J. ZABIEROWSKI⁹

Received 2003 December 14; accepted 2004 May 19

ABSTRACT

The flux of cosmic-ray-induced single hadrons near sea level has been measured with the large hadron calorimeter of the KASCADE experiment. The measurement corroborates former results obtained with detectors of smaller size if the enlarged veto of the 304 m² calorimeter surface is accounted for. The program CORSIKA/QGSJET is used to compute the cosmic-ray flux above the atmosphere. Between $E_0 = 300$ GeV and 1 PeV the primary proton spectrum can be described with a power law parameterized as $dJ/dE_0 = (0.15 \pm 0.03)E_0^{-2.78 \pm 0.03}$ m⁻² s⁻¹ sr⁻¹ TeV⁻¹. At the lower energy end the proton flux compares well with the results from recent direct measurements.

Subject heading: cosmic rays

1. INTRODUCTION

The “knee” in the cosmic-ray energy spectrum has been observed by many research groups and in several observables of air shower experiments. Typically, its position is found around a primary particle energy of 4 PeV. Many theoretical approaches to explain the knee exist. The most probable cause seems to be a superposition of spectra of many nuclei, each with an individual flux cutoff at different energies. The hypotheses of the origin and experimental findings, however, differ significantly, in particular for the primary proton spectrum, which is of special relevance to our understanding of cosmic-ray acceleration and propagation in the Galaxy. Different researchers have claimed to see a proton knee at different energies, e.g., at 10 TeV by the MUBEE collaboration (Zatsepin et al. 1993), at 100 TeV by the Tibet group (Amenomori et al. 2000), and at 4 PeV by the KASCADE collaboration (Ulrich et al. 2001). Taking the experimental data of older direct measurements by balloon or satellite experiments above the atmosphere at face value, one might imagine a change of the power-law slope at 10 TeV. However, recent measurements do not seem to confirm such conjectures. Precise measurements during recent years in the 100 GeV region yielded proton fluxes lower by ~30% than older measurements, e.g., the new data of the BESS (Sanuki et al. 2000), CAPRICE (Mocchiutti et al. 2001), IMAX (Menn et al. 2000), and AMS (Alcaraz et al. 2000) collaborations. On

the other hand, in the 100 TeV region recent publications on direct measurements report higher flux values, e.g., JACEE (Asakimori et al. 1998) and RUNJOB (Apanasenko et al. 2001). These findings indicate that the proton flux does not seem to decrease as strongly as anticipated so far.

It is therefore of interest to determine the proton flux over a wide range of primary energies using one single method. Such a method is the detection of single hadrons at ground level. These unaccompanied hadrons turn out to be intimately connected to primary protons. The latter penetrate deeper into the atmosphere with their hadronic component than heavier primaries of the same energy and are the most abundant producers of single hadrons. Single-hadron spectra have been measured using different experimental techniques, such as emulsion chambers, magnetic spectrometers, and calorimeters. In the past, measurements have been carried out both at sea level (Cowan & Matthews 1971; Siohan et al. 1977; Fickle & Lamb 1979; Mielke et al. 1994) and at mountain altitudes (Aglietta et al. 2003; Inoue et al. 1997). Different definitions of single hadrons are used in the literature. For the present investigations a large calorimeter is used at sea level, and single hadrons are defined as only one hadron with an energy of at least 100 GeV that is reconstructed in the detector. In addition, the zenith angles are restricted to less than 30° in the analysis. During recent years the simulation of air showers has improved considerably, and the primary particle spectra can be deduced from ground-based experiments with more confidence.

The KASCADE calorimeter has been operating continuously and steadily for many years. Large data sets have been accumulated that allow us to estimate the flux up to the PeV range. However, as air shower simulations indicate, more and more single hadrons turn out to originate from higher mass primaries with increasing energy. Hence, the connections to primary protons become less stringent.

2. EXPERIMENTAL APPARATUS

The hadrons have been detected with the central calorimeter of the KASCADE experiment measuring cosmic rays near sea

¹ Institut für Experimentelle Kernphysik, Universität Karlsruhe, 76021 Karlsruhe, Germany.

² Institut für Kernphysik, Forschungszentrum Karlsruhe, 76021 Karlsruhe, Germany.

³ On leave of absence from National Institute of Physics and Nuclear Engineering, 7690 Bucharest, Romania.

⁴ National Institute of Physics and Nuclear Engineering, 7690 Bucharest, Romania.

⁵ Cosmic Ray Division, Yerevan Physics Institute, Yerevan 36, Armenia.

⁶ Current address: Universität Wuppertal, 42119 Wuppertal, Germany.

⁷ Corresponding author; mueller@ik.fzk.de.

⁸ On leave of absence from Moscow State University, 119899 Moscow, Russia.

⁹ Soltan Institute for Nuclear Studies, 90950 Lodz, Poland.

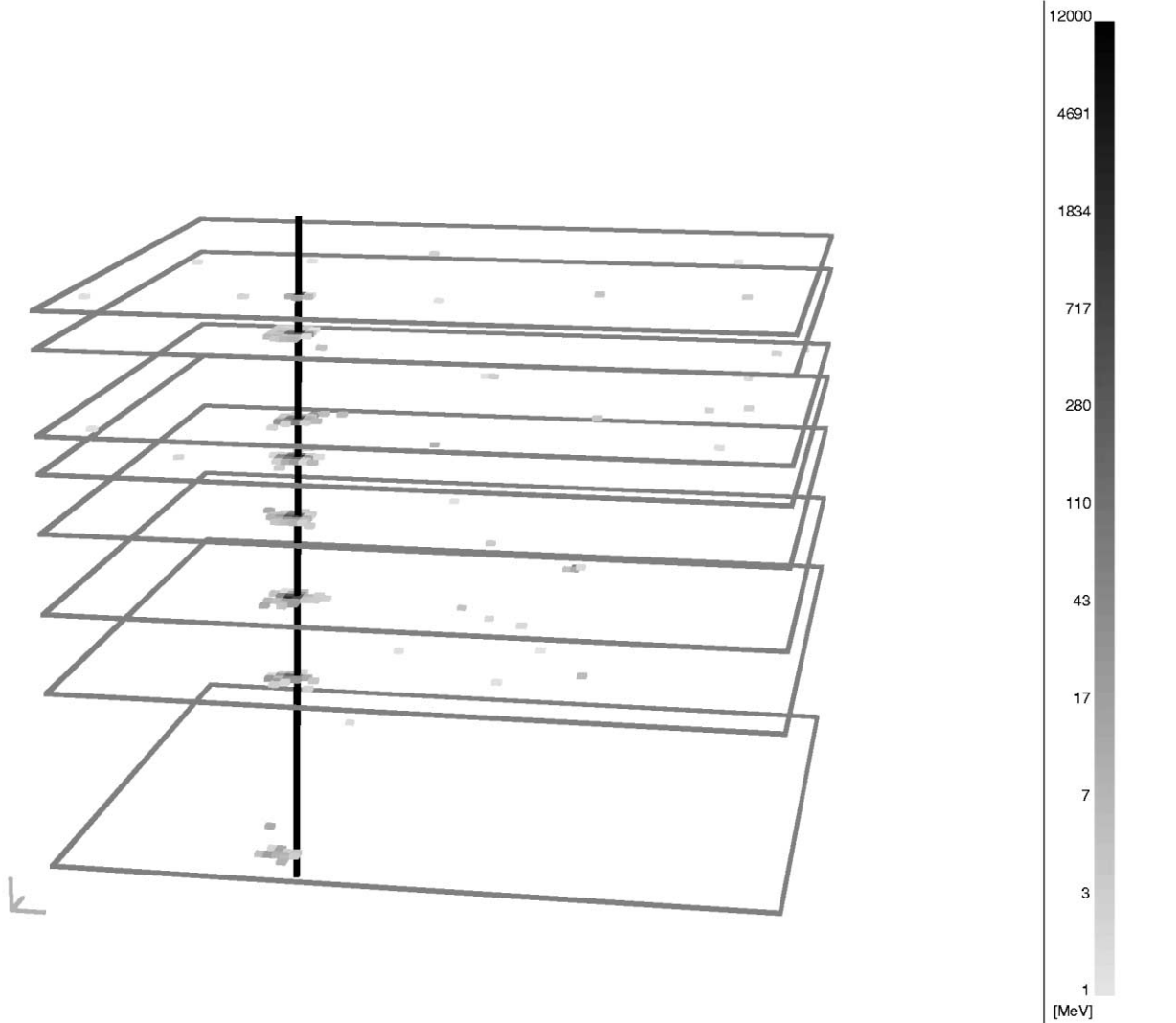


FIG. 1.—Pattern of a single-hadron event in the calorimeter. Each pixel represents the deposited energy on an electrode of $25 \times 25 \text{ cm}^2$. The straight line indicates the reconstructed shower axis.

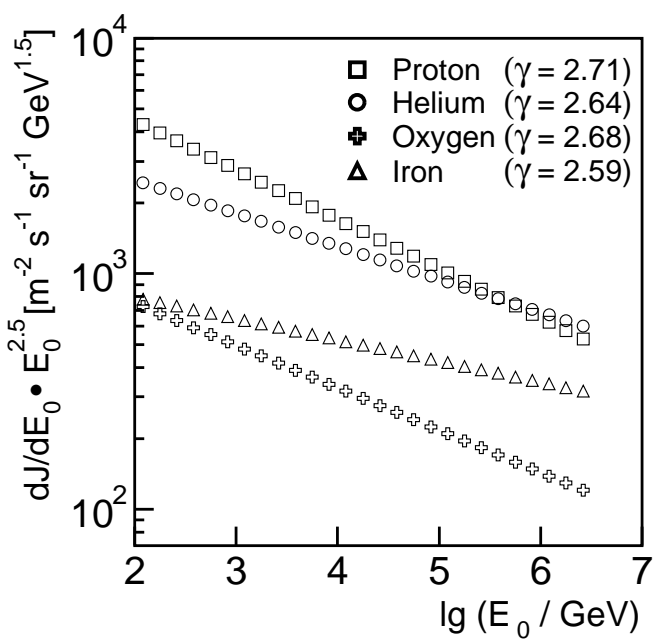


FIG. 2.—Primary flux values for the indicated nuclei vs. the primary particle energy, according to parametrizations for oxygen (Wiebel-Sooth et al. 1998) and for protons, helium, and iron (Hörandel 2003). The corresponding spectral indices γ are given.

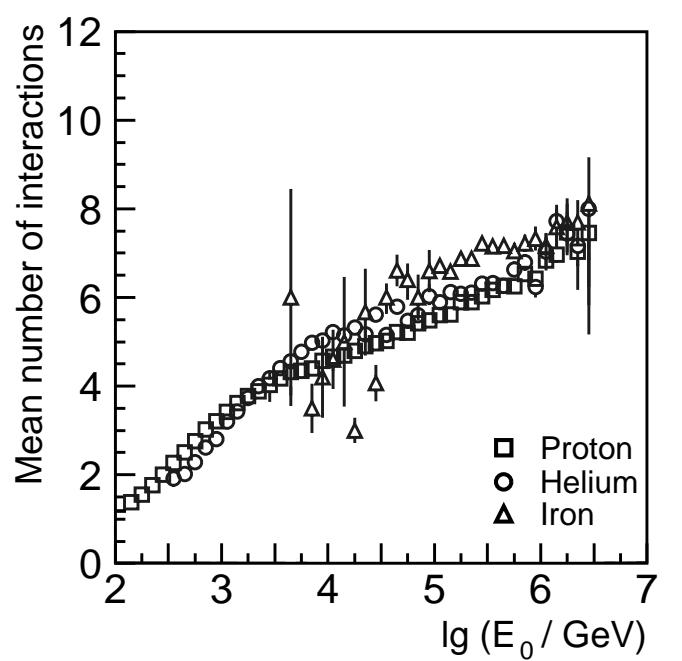


FIG. 3.—Mean number of hadronic interactions in single-hadron events vs. the primary energy for three primary particles as indicated.

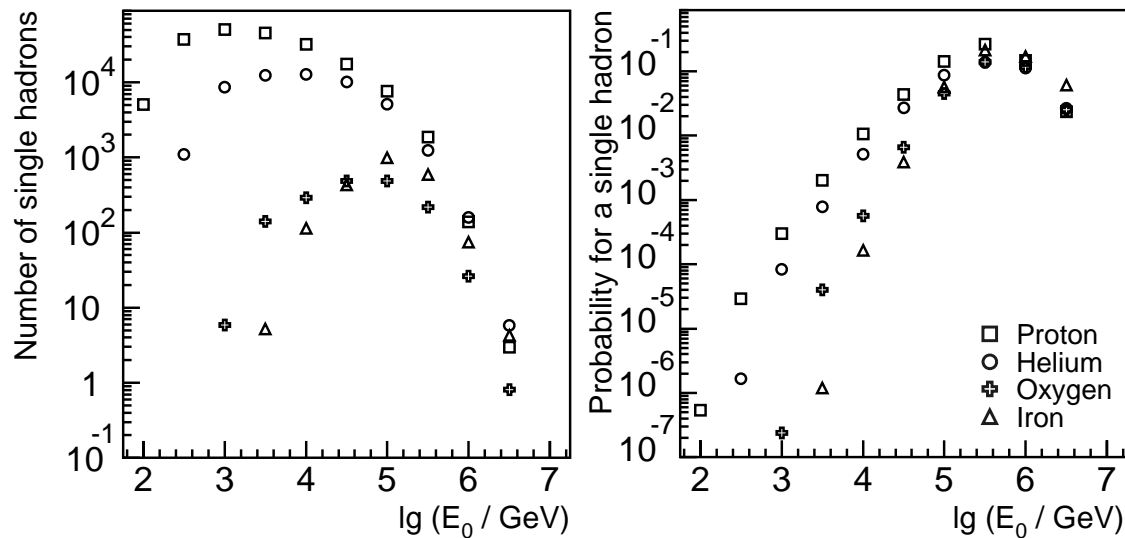


FIG. 4.—Number of reconstructed single-hadron events in the simulations vs. primary energy for the indicated nuclei (*left*). The probability of finding a single hadron vs. primary energy is shown in the right-hand panel.

level (Engler et al. 1999). This is a sampling calorimeter consisting of layers of lead, iron, and concrete absorbers interspersed with nine layers of warm-liquid ionization chambers with an acceptance area of 304 m². The finely segmented chambers allow us to measure the energy of individual hadrons and to reconstruct their point and angle of incidence. An example of a single-hadron event is presented in Figure 1. The energy depositions in the ionization chambers are plotted, from which a total energy of 4.5 TeV for the hadron shown has been reconstructed. Apart from the hadron cascade, no significant energy deposition is seen in the calorimeter layers. In particular, the uppermost layer, where the entire electromagnetic energy is measured, is nearly empty. The detection and reconstruction efficiencies of hadronic cascades in the calorimeter have been determined by simulating cascades with the detector simulation code GEANT¹⁰/FLUKA (Aarnio et al. 1987, 1990). At 100 GeV a trigger and reconstruction efficiency of 50% is reached, increasing to more than 70% at 500 GeV. Radiating muons can imitate a hadron. However, above 100 GeV the

contributions of muons imitating hadrons is below the 1% level (for a detailed discussion see Mielke et al. 1994). The maximum detected energy of an unaccompanied hadron was 50 TeV. During 5 yr of operation (1996–2001), more than 1.5×10^7 events with at least one reconstructed hadron have been recorded, of which 2.5×10^6 had one hadron only.

The calorimeter is surrounded by an array of stations equipped with scintillators in which the electromagnetic and muonic components of an air shower are detected. A description of the experiment can be found in Antoni et al. (2003).

3. SIMULATIONS

The measurements have been accompanied by extensive shower simulations in order to understand the phenomenon of single hadrons and to determine the relation between the primary proton spectrum and the single-hadron spectrum at ground level. The program CORSIKA version 6.014 (Heck et al. 1998) has been employed, with the code QGSJET 01 (Kalmykov & Ostapchenko 1993; Kalmykov et al. 1997; Heck et al. 2001) for high-energy hadronic interactions and GHEISHA (Fesefeldt 1985) for energies below 80 GeV.

For the primary fluxes of nuclei above the atmosphere, parameterizations according to power laws are taken from

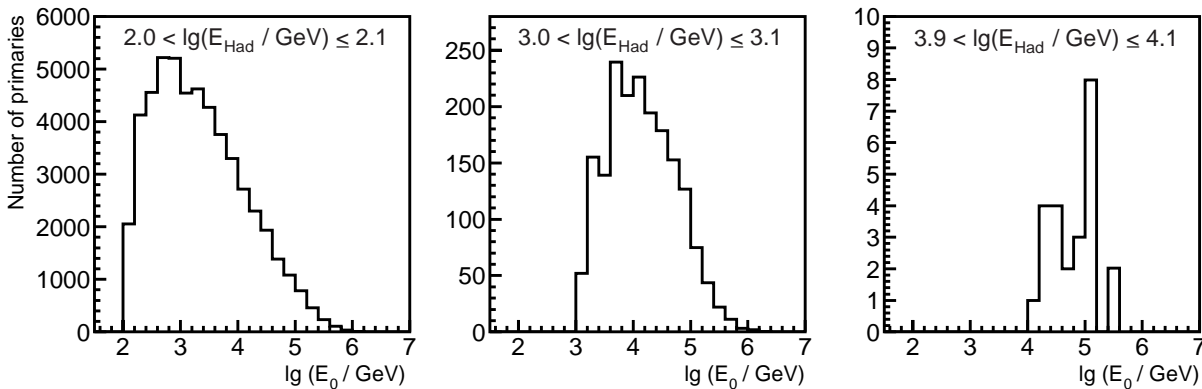


FIG. 5.—Frequency distributions of primary energies for three intervals of single-hadron energies. Simulations with CORSIKA/QGSJET for proton initiated showers are used.

TABLE 1

SINGLE HADRON FLUXES FROM THE VERTICAL DIRECTION MEASURED AT SEA LEVEL

$\log(E_{\text{Had}}/\text{GeV})$	Number of Hadrons	Hadron Flux ($\text{m}^{-2} \text{s}^{-1} \text{sr}^{-1} \text{GeV}^{-1}$)
2.1.....	834920	$(0.20 \pm 0.03) \times 10^{-5}$
2.3.....	693430	$(0.71 \pm 0.11) \times 10^{-6}$
2.5.....	481890	$(0.26 \pm 0.04) \times 10^{-6}$
2.7.....	252110	$(0.79 \pm 0.12) \times 10^{-7}$
2.9.....	113930	$(0.21 \pm 0.04) \times 10^{-7}$
3.1.....	39510	$(0.44 \pm 0.10) \times 10^{-8}$
3.3.....	13220	$(0.89 \pm 0.22) \times 10^{-9}$
3.5.....	4400	$(0.18 \pm 0.04) \times 10^{-9}$
3.7.....	1515	$(0.37 \pm 0.10) \times 10^{-10}$
3.9.....	450	$(0.70 \pm 0.17) \times 10^{-11}$
4.1.....	145	$(0.14 \pm 0.04) \times 10^{-11}$
4.3.....	23	$(0.12 \pm 0.04) \times 10^{-12}$
4.5.....	4	$(0.11 \pm 0.07) \times 10^{-13}$
4.7.....	2	$(0.24 \pm 0.32) \times 10^{-14}$

NOTE.—Errors represent systematic uncertainties.

compilations by Wiebel-Sooth et al. (1998) and Hörandel (2003). In the latter review more recent measurements are taken into account and the parameterizations for protons, helium, and iron have been updated. In total, $\sim 2 \times 10^{10}$ events have been simulated in the energy range from 100 GeV to 3 PeV for proton-, helium-, oxygen-, and iron-induced showers. The number corresponds to a data-taking period of approximately 80 days for the calorimeter acceptance. For illustration, the fluxes used are depicted in Figure 2, marked with the corresponding spectral index γ and extrapolated into the PeV region. The shower cores of the simulated events have been distributed evenly over the calorimeter area, extended by 2 m at all four sides. The hadrons are tightly concentrated near the shower axis. The simulated distance distribution can be parameterized by an exponential function that falls off to $1/e$ within 4.3 m, nearly independent of energy. Using this lateral distribution, calculations show that out of all primary particles, which are reconstructed as single hadrons, 75% have been simulated. The simulations reveal, however, that for a given interval of hadron energy the fraction of missing events is nearly independent of primary energy. Since the missing percentage does not depend strongly on energy, it has no significant effect on the deduced primary proton spectrum, which is presented in § 5.

Single hadrons belong to a particular class of air showers for which the detected hadrons stem from air showers with only a few interactions in the atmosphere. In the vertical direction the thickness of the atmosphere corresponds to ~ 11 interaction lengths. The number of hadronic interactions occurring for single-hadron events is shown in Figure 3. In the TeV range primary protons or helium nuclei encounter three or four interactions only. Integrated over all relevant energies, the average number of interactions is 3.6 for primary protons. Heavier nuclei do not generate single hadrons in this energy range, as revealed by the primary iron simulations. Oxygen and iron nuclei can be seen in this class of events only if the primaries have energies higher than 30 TeV.

The number of reconstructed single-hadron events for the four classes of primaries are shown in the left-hand panel of Figure 4. In the right-hand panel the corresponding probability of finding a single-hadron event is plotted for primaries with respect to their energy. One can see that up to a few TeV,

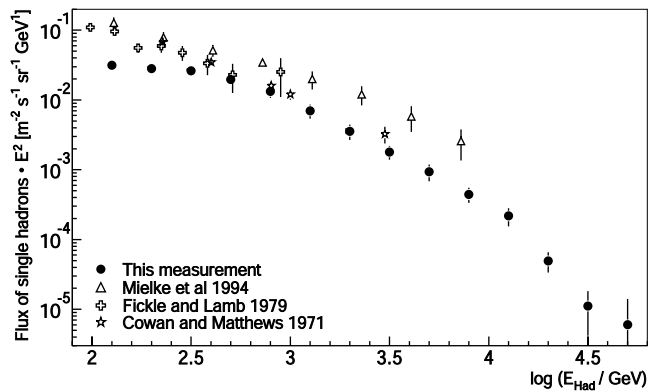


FIG. 6.—Single hadron spectrum: flux multiplied by the energy squared vs. single-hadron energy. For comparison, results from other experiments near sea level are presented.

indeed, single hadrons originate mostly from primary protons and that above 10 TeV helium primaries also contribute. At approximately 1 PeV, protons and helium contribute with equal numbers to single hadrons, and at higher energies heavier nuclei also have to be considered. The right-hand panel reveals that in the 100 TeV range, 10% of all showers are of the single-hadron type. This figure is valid for the present definition of a single hadron. If accompanying electromagnetic energy also excluded single hadrons they would be encountered less frequently, as outlined in the next section.

The simulations show how closely the single-hadron events are related to the primary particles. In Figure 5 the distributions of primary proton energies are presented for three energy bins of single hadrons, ~100 GeV, 1 TeV, and 10 TeV. The spread of the primary energy is wide, but the bulk of parents have an energy 10 times larger than the observed energy for all three intervals. Based on simulations, it has been verified that the 25% of events that are missing do not change the shape of the distributions appreciably. Therefore, despite the large fluctuations, measuring the single-hadron spectrum allows us to deduce the primary proton flux.

4. SINGLE-HADRON SPECTRUM

The flux of single hadrons is obtained using the trigger and reconstruction efficiencies, as determined with the GEANT/FLUKA code. The data are given in Table 1 and Figure 6. The errors quoted are estimated systematic uncertainties concerning the fiducial area of the calorimeter, the total data taking time, the effective solid angle, and the energy assignment, but are dominated by the trigger and reconstruction efficiencies. They amount to approximately 15% below 1 TeV, 25% in the TeV range, and 35% above 10 TeV. The numbers of collected hadrons given in the table indicate that statistical errors can be neglected below 10 TeV. The data exhibit almost a power law in the double logarithmic graph. However, on the energy scale of over 2.5 orders of magnitude a gentle bend is apparent. Such behavior is also observed in the simulations. For reference, measurements from the literature (Cowan & Matthews 1971; Fickle & Lamb 1979) are shown, as well as the data from the KASCADE prototype calorimeter (Mielke et al. 1994). The last experiment exhibits somewhat larger fluxes compared with the present data because of its smaller surface of 6 m^2 . The KASCADE calorimeter, with a 304 m^2 fiducial area, has a more efficient veto for multiple hadron detection. Especially for low hadron energies, this may cause the differences. The data of the

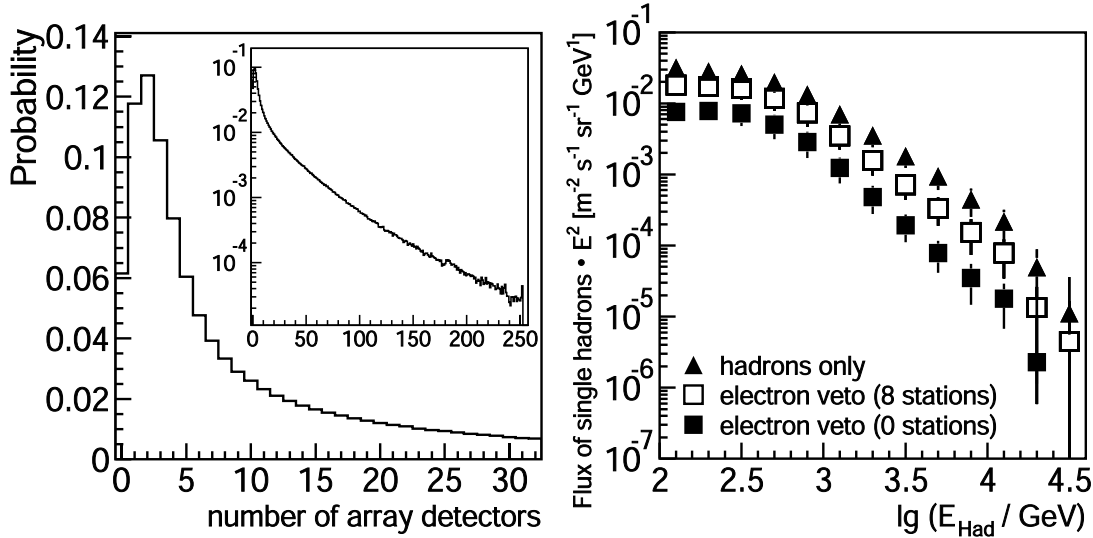


FIG. 7.—Left: Number of electromagnetic detectors with $E_{\text{dep}} \geq 5$ MeV. Right: Single-hadron spectrum compared with additional vetos: not more than eight array stations or no station have registered a minimum ionizing particle. The ordinate has been multiplied by the energy squared.

two older experiments, which both had smaller apertures of $\sim 0.65 \text{ m}^2 \text{ sr}$, show a similar shape.

Also, in the present investigations, accompanying electromagnetic radiation detected in the scintillators of the array stations can be accounted for. The graph in the left-hand panel of Figure 7 shows the number of stations that have registered at least one minimum ionizing particle in coincidence with a single hadron. In fact, only 6% of the single-hadron events are not accompanied by a signal in the array stations. As can be inferred from the insert, a small probability exists that all 252 array stations have a signal in coincidence with a single hadron. All this signifies that the notion of the “single hadron” is somewhat artificial; it depends on the experimental conditions and ipso facto changes from experiment to experiment. Demanding that not more than eight stations have an electronic signal, i.e., $E_{\text{dep}} \geq 5$ MeV, already reduces the number of single-hadron events by $\frac{1}{3}$. This can be seen in the right-hand panel of Figure 7, where the single-hadron spectrum is compared with this additional requirement. One observes that the electron veto becomes stronger for large hadron energies, which in the mean originate from higher primary energies. Simulations indicate that the sensitivity to primary protons is also enhanced. In the figure, the flux with no signal at all in the 252 stations is presented as well. However, because the number of events fulfilling this requirement is too small, the veto condition of not more than eight stations activated has been chosen for further analyses, in particular when deducing the primary proton spectrum.

5. PRIMARY PROTON SPECTRUM

The single-hadron spectrum is converted to a flux of primary protons by attributing to the measured hadrons a probable primary energy according to the energy distributions illustrated in Figure 5. In principle, the single-hadron spectrum $g(\log E_{\text{Had}})$ has to be converted to a flux of primary protons $f(\log E_0)$ by solving the integral equation

$$g(\log E_{\text{Had}}) = \int A(\log E_{\text{Had}} | \log E_0) f(\log E_0) d \log E_0. \quad (1)$$

$A(\log E_{\text{Had}} | \log E_0)$ is the transfer function transforming the primary flux spectrum into the measured single-hadron spectrum

at ground level, accounting for the interactions in the atmosphere. Several methods exist to deconvolute one-dimensional spectra. For the sake of simplicity, a slightly different approach has been chosen, which turned out to be rather robust and straightforward. Knowing the probability density distribution $B(\log E_0 | \log E_{\text{Had}})$ for a given single-hadron energy $\log E_{\text{Had}}$, the primary proton flux can be inferred by

$$f(\log E_0) = \int B(\log E_0 | \log E_{\text{Had}}) g(\log E_{\text{Had}}) d \log E_{\text{Had}}. \quad (2)$$

Using the calculated probability distributions (see, e.g., Fig. 5), assuming primary fluxes as given in Figure 2, the primary proton flux is obtained. The resulting energy spectrum depends only slightly on the slope of the a priori flux assumptions, as can be seen in Figure 8. Plotted are the power-law indices derived from the data versus the assumed indices in the

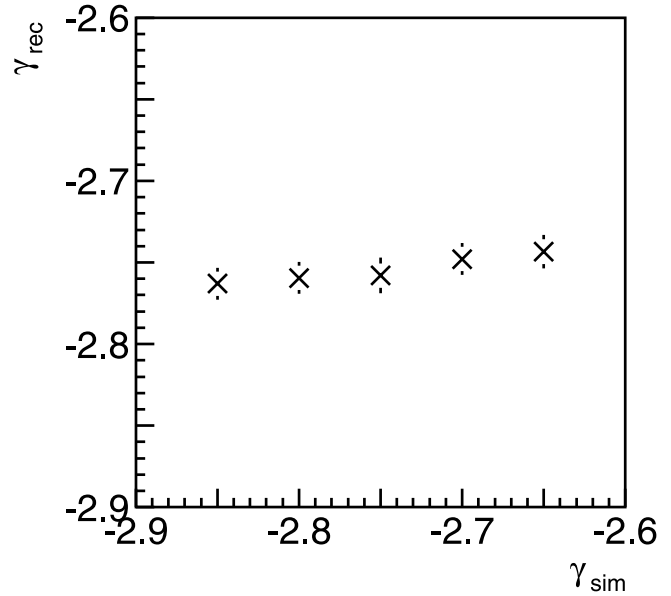


FIG. 8.—Spectral index of the primary proton spectrum deduced from the measurements vs. the slope used in the simulations of the probability density distributions.

TABLE 2

PRIMARY FLUX OF PROTONS DEDUCED FROM THE SINGLE-HADRON SPECTRUM

Primary Energy E_0 [log(E_0/GeV)]	Uncorrected Flux $\times E_0^{2.5}$ ($\text{m}^{-2} \text{s}^{-1} \text{sr}^{-1} \text{GeV}^{1.5}$)	Proton Flux $\times E_0^{2.5}$ ($\text{m}^{-2} \text{s}^{-1} \text{sr}^{-1} \text{GeV}^{1.5}$)
2.5.....	4680 \pm 1025 (± 700)	4675 \pm 1025 (± 700)
3.0.....	3800 \pm 830 (± 550)	3400 \pm 740 (± 500)
3.5.....	3000 \pm 660 (± 450)	2470 \pm 545 (± 370)
4.0.....	2330 \pm 500 (± 355)	1800 \pm 395 (± 270)
4.5.....	1900 \pm 565 (± 490)	1310 \pm 385 (± 330)
5.0.....	1520 \pm 450 (± 385)	950 \pm 285 (± 240)
5.5.....	1040 \pm 420 (± 370)	690 \pm 280 (± 240)
6.0.....	775 \pm 310 (± 285)	505 \pm 200 (± 180)

NOTE.—Primary flux of protons deduced from the single-hadron spectrum, assuming protons only (second column), and with contributions from helium and heavy nuclei subtracted (third column). The errors are systematic uncertainties (in parentheses are the contributions from the systematic errors of the single-hadron spectrum).

simulations of the probability distributions. One realizes that the method yields rather stable results.

The outcome for the uncorrected primary fluxes are given in the second column of Table 2, assuming that all primaries are protons. They are multiplied by $E^{2.5}$ in order to compensate the steeply falling power-law spectrum. As seen in Figure 4, at higher energies helium and to some extent the heavier nuclei also initiate single-hadron events. These contributions are subtracted by taking into account the parameterized primary fluxes as shown in Figure 2. The final proton fluxes are presented in the third column. In the TeV region the difference of the flux values amounts to $\sim 20\%$, a value comparable to the errors as discussed in the following.

The errors quoted are estimates of systematic uncertainties. They include the calculation of the probability density distribution and the errors in the single-hadron spectrum (given in parentheses), both added quadratically. The uncertainties in

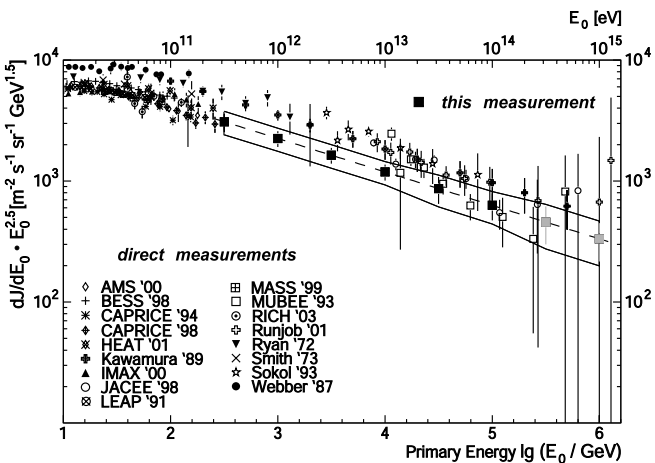


FIG. 9.—Flux of primary protons as a function of energy (black- and gray-shaded squares). The dashed line represents a fit of a power law. The lines indicate the maximum systematic errors estimated. For comparison, results of direct measurements are shown: AMS (Alcaraz et al. 2000), BESS (Sanuki et al. 2000), CAPRICE 94 (Boezio et al. 1999), CAPRICE 98 (Mocchiutti et al. 2001), HEAT (DuVernois et al. 2001), Kawamura et al. (1989), IMAX (Menn et al. 2000), JACEE (Asakimori et al. 1998), LEAP (Seo et al. 1991), MASS (Bellotti et al. 1999), MUBEE (Zatsepin et al. 1993), RICH (Diehl et al. 2003), RUNJOB (Apanasenko et al. 2001), Ryan et al. (1972), Smith et al. (1973), Sokol (Ivanenko et al. 1993), and Webber et al. (1987).

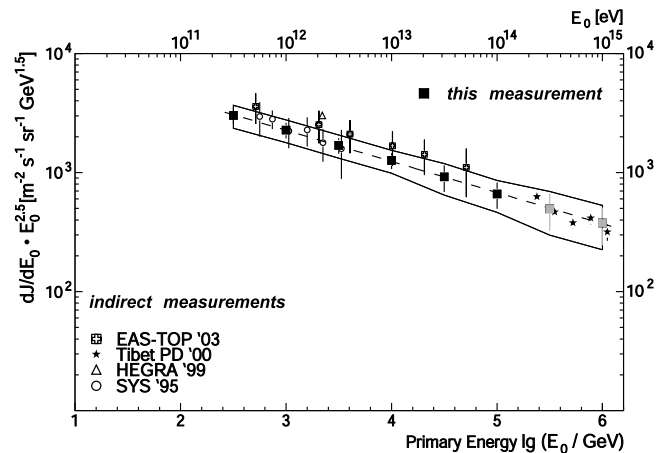


FIG. 10.—Flux of primary protons as presented in Fig. 9. For comparison, results of indirect measurements by air shower are shown: EAS-TOP (Aglietta et al. 2003), Tibet (Amenomori et al. 2000), HEGRA (Aharonian et al. 1999), and SYS (Inoue et al. 1997).

$B(\log E_0 | \log E_{\text{Had}})$ are estimated to amount to 15% below a few TeV and 20% at higher values of E_0 .

Graphic representations of the results are shown in Figures 9 and 10. The present data are plotted as filled squares, and the maximal errors are indicated by the two lines. The error bars on the individual points represent the systematic uncertainties in the single-hadron flux. The squares follow a power law reasonably well; a corresponding fit yields $dJ/dE_0 = (0.15 \pm 0.03)E_0^{-2.78 \pm 0.03} \text{ m}^{-2} \text{ s}^{-1} \text{ sr}^{-1} \text{ TeV}^{-1}$, which is indicated by the dashed line. It should be kept in mind that for higher energies above 100 TeV, contributions of helium and heavy nuclei of up to 50% had to be subtracted. In the figures the corresponding values are marked as shaded points.

In Figure 9 the data are compared with results of direct measurements above the atmosphere taken from the literature. One can recognize differences between the individual results of the order of a factor of 2. Within these uncertainties the present data are compatible with results from the literature. At energies around 100 GeV the most recent data of direct measurements scatter at the lower bound of the published fluxes. Our proton flux extrapolates well to these data. This fact can be interpreted in such a way that in this energy region from 10^2 to 10^4 GeV the hadronic shower cascade within the atmosphere is well described by the program CORSIKA with the interaction code QGSJET 01. In addition, other tests have proven that below 1 PeV the latter code describes the shower propagation best (Antoni et al. 1999, 2001).

In Figure 10 our data are shown, together with fluxes for primary protons obtained by experiments, using indirect methods of measurements as well. Within the errors given, the data corroborate previous measurements.

6. SUMMARY

Using the large hadron calorimeter of the KASCADE experiment during 3 yr of effective data taking, 2.5×10^6 events have been accumulated for which a single hadron was reconstructed. With these data, the energy spectrum of single hadrons has been derived. These data are somewhat lower than fluxes published previously. This is attributed to the large surface area of the calorimeter, which acts as a more efficient veto against multihadron events.

Single-hadron events are particular air showers, which predominantly stem from primary protons in the energy region considered. Applying large sets of simulated single-hadron events, probability distributions for the corresponding primary energy have been obtained up to the PeV region, and the primary spectrum for protons could be determined. The data extend over nearly 4 orders of magnitude in primary energy and can be described by a power law with a flux parameterized as $dJ/dE_0 = (0.15 \pm 0.03)E_0^{-2.78 \pm 0.03} \text{ m}^{-2} \text{ s}^{-1} \text{ sr}^{-1} \text{ TeV}^{-1}$.

The authors would like to thank the members of the engineering and technical staff of the KASCADE collaboration, who contributed with enthusiasm and commitment to the success of the experiment. The KASCADE experiment is supported by the German Federal Ministry of Education and Research and was embedded in collaborative WTZ projects between Germany and Romania (RUM 97/014) and Poland (POL 99/005) and Armenia (ARM 98/002). The Polish group acknowledges the support by KBN grant 5PO3B 13320.

REFERENCES

- Aarnio, P. A., et al. 1987, FLUKA Users Guide, Technical Report TIS-RP-190 (Geneva: CERN)
 ———. 1990, FLUKA Users Guide, Technical Report TIS-RP-190 (Geneva: CERN)
 Aglietta, M., et al. 2003, Astropart. Phys. 19, 329
 Aharonian, F., et al. 1999, Phys. Rev. D, 59, 092003
 Alcaraz, J., et al. 2000, Phys. Lett. B, 490, 27
 Amenomori, M., et al. 2000, Phys. Rev. D, 62, 112002
 Antoni, T., et al. 1999, J. Phys. G, 25, 2161
 ———. 2001, J. Phys. G, 27, 1785
 ———. 2003, Nucl. Instrum. Methods A, 513, 490
 Apanasenko, A. V., et al. 2001, Astropart. Phys., 16, 13
 Asakimori, K., et al. 1998, ApJ, 502, 278
 Bellotti, R., et al. 1999, Phys. Rev. D, 60, 052002
 Boezio, M., et al. 1999, ApJ, 518, 457
 Cowan, E. W., & Matthews, K. 1971, Phys. Rev. D, 4, 37
 Diehl, E., et al. 2003, Astropart. Phys., 18, 487
 DuVernois, M. A., et al. 2001, Proc. 27th Int. Cosmic Ray Conf. (Hamburg), 5, 1618
 Engler, J., et al. 1999, Nucl. Instrum. Methods A, 427, 528
 Fesefeldt, H. 1985, The Simulation of Hadronic Showers: Physics and Applications (Aachen: RWTH)
 Fickle, R. K., & Lamb, R. C. 1979, Nuovo Cimento Lett., 25, 289
 Heck, D., et al. 1998, CORSIKA: A Monte Carlo Code to Simulate Extensive Air Showers (FZKA 6019; Karlsruhe: Forschungszentrum Karlsruhe)
 ———. 2001, Proc. 27th Int. Cosmic Ray Conf. (Hamburg), 1, 233
 Hörandel, J. R., 2003, Astropart. Phys., 19, 193
 Inoue, N., et al. 1997, Proc. 25th Int. Cosmic Ray Conf. (Durban), 4, 113
 Ivanenko, I. P., et al. 1993, Proc. 23rd Int. Cosmic Ray Conf. (Calgary), 2, 17
 Kalmykov, N. N., Ostapchenko, S. S. 1993, Yad. Fiz., 56, 105
 Kalmykov, N. N., et al. 1997, Nucl. Phys. B, 52, 17
 Kawamura, Y., et al. 1989, Phys. Rev. D, 40, 729
 Menn, W., et al. 2000, ApJ, 533, 281
 Mielke, H. H., et al. 1994, J. Phys. G, 20, 637
 Mocchiatti, E., et al. 2001, Proc. 27th Int. Cosmic Ray Conf. (Hamburg), 5, 1634
 Ryan, M. J., et al. 1972, Phys. Rev. Lett., 28, 985
 Ulrich, H., et al. 2001, Proc. 27th Int. Cosmic Ray Conf. (Hamburg), 1, 97
 Sanuki, T., et al. 2000, ApJ, 545, 1135
 Seo, E. S., et al. 1991, ApJ, 378, 763
 Siohan, F., et al. 1977, J. Phys. G, 3, 1157
 Smith, L. H., et al. 1973, ApJ, 180, 987
 Webber, W. R., et al. 1987, Proc. 20th Int. Cosmic Ray Conf. (Moscow), 1, 325
 Wiebel-Sooth, B., et al. 1998, A&A, 330, 389
 Zatsepin, V. I., et al. 1993, Proc. 23rd Int. Cosmic Ray Conf. (Calgary), 2, 13